Nanotechnology **19** (2008) 145302 (6pp) doi:10.1088/0957-4484/19/14/145302

Fabrication of large area nanoprism arrays and their application for surface enhanced Raman spectroscopy

B Cui, L Clime, K Li and T Veres

Industrial Materials Institute, National Research Council of Canada, 75 de Mortagne Blvd, Boucherville, QC, J4B6Y4, Canada

E-mail: teodor.veres@imi.cnrc-nrc.gc.ca

Received 29 November 2007, in final form 29 January 2008
Published 4 March 2008
Online at stacks.iop.org/Nano/19/145302

Abstract

This work demonstrates the fabrication of metallic nanoprism (triangular nanostructure) arrays using a low-cost and high-throughput process. In the method, the triangular structure is defined by the shadow of a pyramid during angle evaporation of a metal etching mask. The pyramids were created by nanoimprint lithography in polymethylmethacrylate (PMMA) using a mould having an inverse-pyramid-shaped hole array formed by KOH wet etching of silicon. Silver and gold nanoprism arrays with a period of 200 nm and an edge length of 100 nm have been fabricated and used as effective substrates for surface enhanced Raman spectroscopy (SERS) detection of rhodamine 6G (R6G) molecules. Numerical calculations confirmed the great enhancement of electric field near the sharp nanoprism corners, as well as the detrimental effect of the chromium adhesion layer on localized surface plasmon resonance. The current method can also be used to fabricate non-equilateral nanoprism and three-dimensional (3D) nanopyramid arrays, and it can be readily extended to other metals.

(Some figures in this article are in colour only in the electronic version)

1. Introduction

Triangular nanostructures (nanoprisms) have demonstrated interesting plasmonic properties. The localized surface plasmon resonance (LSPR) spectra can be tuned systematically over a large range by varying the size, shape and height of the nanoprisms [1]. At the sharp corners, they have shown to exhibit a strong local electromagnetic field enhancement due to the lightning rod effect [2]. Both tunability and high local electromagnetic field enhancement are very important in chemical or biological sensing applications based on surface enhanced Raman spectroscopy (SERS) [3, 4]. Moreover, thin nanoprisms have a high sensing volume that makes them suitable for detecting large biomolecules [5].

The nanoprisms are typically fabricated by chemical approaches, either through the chemical reduction of metal salts [6, 7] or through the light-induced aggregation of small nanoparticle seeds [8, 9]. These methods, although capable of producing nanoprisms with sharp corners, lead to disordered systems that cannot be easily used or manipulated for a reproducible and predictable generation of SERS enhancement. Nanolithography is required in order to fabricate a regular array of nanoprisms having homogeneous sizes, shapes, heights and inter-particle distances. Due to their low-throughput, electron-beam lithography or focused ion beam milling are unsuitable for producing nanoprism arrays over a large area at low-cost. Previously, nanosphere lithography (NSL) has been employed to fabricate ordered (equilateral) Ag nanoprism arrays into the gaps between adjacent spheres [1, 10]. However, even though the spheres have a uniform size, any deviation from the perfect arrangement will result in nanoprisms of uncontrolled shapes. In this paper, we report an alternative technique for the fabrication of periodic nanoprism arrays over a large area by nanoimprint lithography (NIL). Unlike the chemical approaches, the current technique can readily be extended to other metals, such as magnetic materials. Compared to NSL, the current method is suitable for the fabrication of smaller nanoprisms (sub-100 nm) in a more compact periodic arrangement. The current method can also produce non-

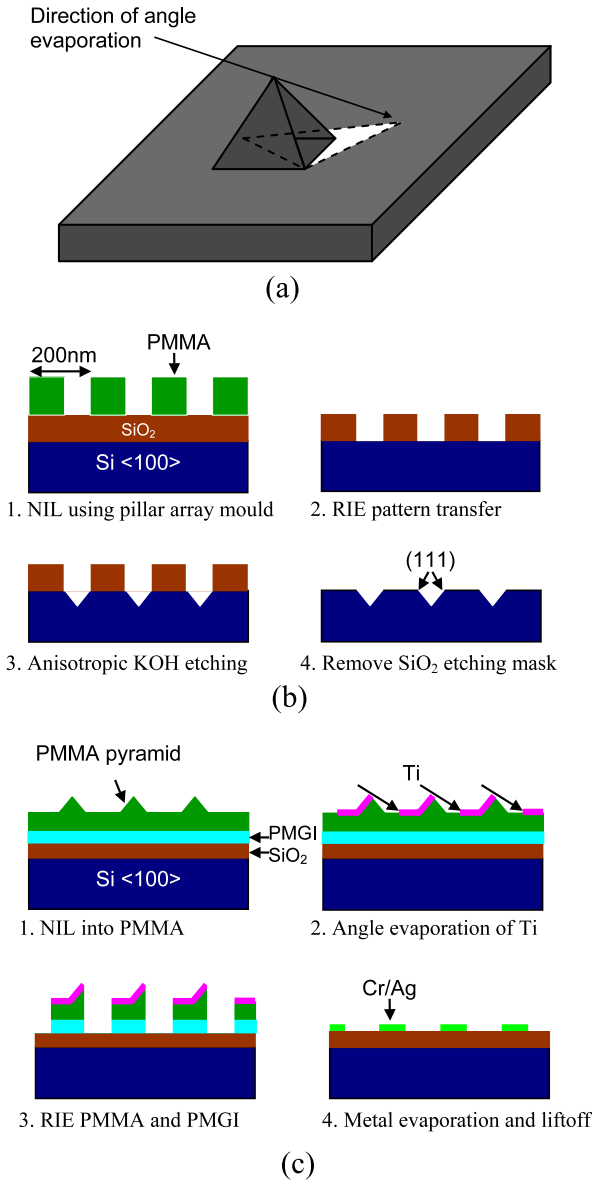

Figure 1. (a) Fabrication principle of a nanoprism (the white area) defined by the shadow of a pyramid during angle evaporation of a metal RIE mask; (b) schematic of the mould fabrication process; (c) schematic of the nanoprism fabrication process.

equilateral nanoprisms that offer an additional degree for tuning and boosting the plasmonic properties.

2. Fabrication

In our method, the triangular structure is defined by the shadow of a pyramid (the white area in figure 1(a)). The process can be divided into two parts: the fabrication of a NIL mould bearing an array of inverse-pyramid-shaped holes (figure 1(b)), and the fabrication of a nanoprism array by NIL using this mould (figure 1(c)). In the mould fabrication, the inverse-pyramid-shaped holes were formed by the ⟨111⟩ crystalline planes of the (100) silicon wafer using anisotropic KOH wet etching of silicon. The wet etching mask contains a 200 nm period cylindrical-shaped hole array in 80 nm-thick SiO_2, and it was fabricated by NIL using a pillar array mould over a 4 inch wafer and reactive ion etching (RIE) pattern transfer to the SiO_2 layer. Before KOH etching, the native oxide layer on silicon was removed by 1:50 diluted HF for 30 s, and the wet etching of Si was carried out using 7.0 wt% KOH at 50 °C for 50 s. After removing the SiO_2 etching mask by HF, the wafer was exposed to oxygen plasma to generate an oxide layer on the silicon surface before anti-stiction treatment using 1H, 1H, 2H, 2H-perfluorooctyl-trichlorosilane. Using this mould, a pyramid array was created by NIL in a polymer resist, here 200 nm PMMA, that was spun on a 70 nm-thick polymethylglutarimide (PMGI) liftoff layer (MicroChem Corp), which was in turn spun on a silicon wafer having 500 nm-thick thermal oxide. The NIL was carried out at 180 °C (below the glass transition temperature of PMGI) and 35 bar for 20 min. Next, angle evaporation of 15 nm Ti was carried out that covered the whole surface area except the shadows of the pyramids (white triangular area in figure 1(a)). The PMMA/PMGI within the triangle was subsequently etched through to the substrate by RIE using an Oxford Instruments PlasmaLab 80Plus etcher with 20 sccm of O_2 gas, a pressure of 10 mTorr and a power of 100 W, which resulted in etching rates of 180 nm min^{-1} and 130 nm min^{-1} for PMMA and PMGI, respectively. We etched the polymer stack for 2.5 min, which led to an undercut profile that facilitated the subsequent liftoff process. PMGI is utilized because it is difficult to dissolve PMMA by solvents once it is exposed to oxygen plasma, making liftoff by PMMA using solvents impractical. Finally, metal nanoprisms were obtained after standard metal evaporation and liftoff using MF-319 developer (Rohm and Haas Electronic Materials) that dissolves PMGI.

The scanning electron microscopy (SEM) image of the mould bearing an inverse-pyramid-shaped hole array is shown in figure 2(a). Figure 2(b) shows an array of 20 nm Ag nanoprisms (with 2.5 nm Cr as adhesion layer) with an edge length of about 100 nm and a period of 200 nm. Here Ti was deposited at a tilt angle of 65° along the diagonal direction of the pyramid base. The corners of the triangles are slightly rounded because: (1) the pyramid apex in PMMA is slightly blunt when imprinted at a finite pressure (apex radius proportional to surface tension/pressure); (2) the pyramid base is not a perfect square and thus the apex is a short line rather than a point; (3) the landed Ti adatoms diffuse before they stop by a short distance that increases with the tilt angle; and (4) the prism's sharp tips were possibly annealed by solvents used in the fabrication process [11]. The base of the triangle (here 100 nm) is determined by the length of the diagonal of the pyramid base square in the mould, while the height can be adjusted by varying the tilt angle of Ti evaporation. An asymmetric triangle or even a quadrangle could be produced by Ti deposition off the diagonal direction of the pyramid base. In addition, three-dimensional nanopyramids can be fabricated by prolonged deposition as the holes become gradually closed by the evaporated material. Figure 2(c) shows an array of nanopyramids after the deposition and liftoff of 5 nm Cr as an adhesion layer and 100 nm Ag.

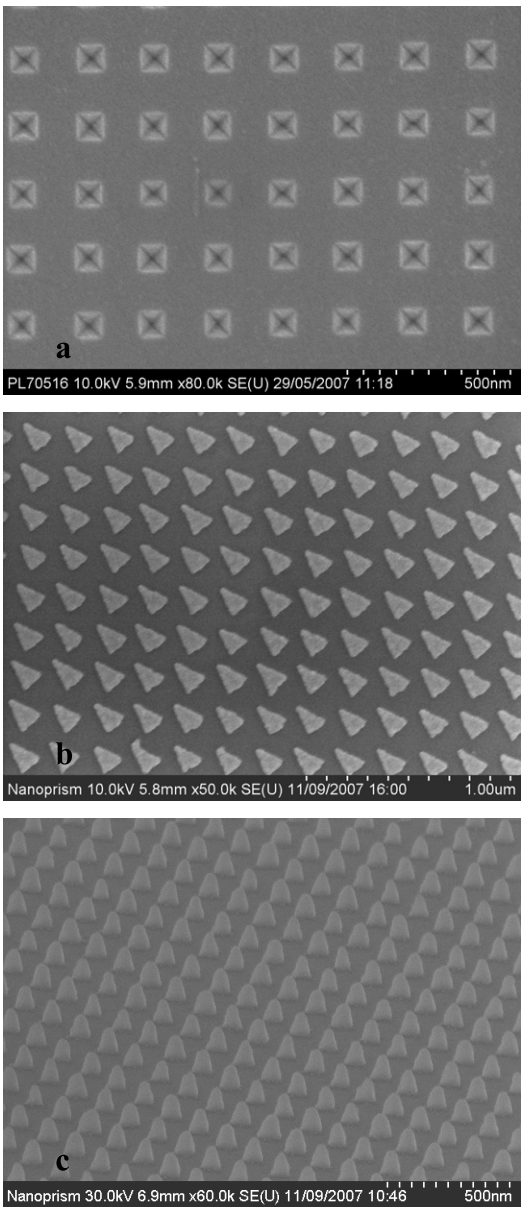

Figure 2. (a) SEM image of the NIL mould with 200 nm period inverse-pyramid-shaped hole array; (b) SEM image of a 200 nm period nanoprism array of 20 nm Ag (with 2.5 nm Cr adhesion layer); (c) SEM image of a nanopyramid array resulting from the evaporation of 100 nm Ag (with 5 nm Cr adhesion layer) and subsequent liftoff. Sample tilted 75° during imaging.

3. Surface enhanced Raman spectroscopy (SERS)

One important application of nanoprism arrays is label-free detection with high sensitivity and spectral specificity of low-abundance chemical and biomolecules based on SERS. As an example, rhodamine 6G (R6G) was adsorbed on the nanoprism array of 20 nm Ag (with 2.5 nm Cr as adhesion layer) by placing a drop of 10^{-5} M solution and letting it dry in air. The Raman spectra were acquired by using a micro-Raman station from Avalon Instruments with a laser excitation wavelength of 785 nm, a power of 0.16 mW μm^{-2}, a spot size of 25 μm (objective lens 40×), and a collection time of 3 s. The SERS spectrum of R6G is plotted in figure 3, which shows clearly almost all the characteristic Raman peaks of R6G molecules, as well as that of the bulk silicon (520 cm^{-1}) underneath the transparent SiO_2 layer.

Since noble metals do not adhere well to silicon dioxide, it is important to add an adhesion promotion layer such as Cr before deposition of a noble metal. But the Cr layer would greatly reduce the LSPR because, for strong LSPR, the metal should have a large (negative) real and a small imaginary electric permittivity, which is the case for Ag and Au but not for Cr, whose permittivity presents real and imaginary parts respectively 20 times smaller and 50 times greater than those of Ag at $\lambda = 800$ nm. To study the effect of the Cr adhesion layer, we fabricated three nanoprism arrays: (A) Cr(1 nm)/Au(30 nm); (B) Cr(5 nm)/Au(30 nm); and (C) Cr(4 nm), expose to atmosphere, then deposit Cr(1 nm)/Au(30 nm). Au was chosen here because, unlike Ag, its surface is stable in air, leading to a stable bonding of R6G molecules to the Au surface that is essential for a valid comparison between different samples. R6G was adsorbed on the Au surface by soaking the samples in a 10^{-5} M R6G solution for 30 min, then rinsing briefly with de-ionized water and blow drying with N_2 gas. The coverage of molecular R6G on the Au surface is expected to be a monolayer or less. Five Raman spectra were collected for each sample at random locations, and the counts for the peak at 1180 cm^{-1} were found to vary within 20% for each sample. The average counts at 1180 cm^{-1} are 2600 and 1200 for samples A and C, respectively; and there is no detectable Raman signal from R6G for sample B (figure 4(a)). There is also no detectable Raman signal for the continuous Au film, since it is fairly smooth, even when with only 1 nm of Cr adhesion layer (figure 4(b)). Consequently, the drastic drop in Raman signal when Cr was increased from 1 to 5 nm is mainly due to the intrinsic properties of Cr, as mentioned above, rather than due to surface roughness. Both samples B and C have 5 nm of Cr in total, but the top ∼2 nm of the 4 nm Cr layer for sample C would be oxidized once exposed to air. Therefore, the higher Raman signal for sample C compared to sample B can be explained by the following two factors: the 'effective' Cr thickness for sample C is actually ∼3 nm due to surface oxidation (dominant factor); and the Cr oxide layer might reduce the coupling between Au and the remaining non-oxidized Cr layer underneath. Given the detrimental effect of Cr, it is important to use a very thin (∼1 nm) Cr adhesion layer in order to minimize its effect and thus achieve high SERS enhancement.

4. Numerical calculation of near field and absorption efficiency

The discrete dipole approximation (DDA) [12–15] with a dipole grid length of 3 nm was used to calculate the near field and the absorption efficiency of the nanoprisms. The DDA algorithm is a powerful approach for computing the scattering of light by wavelength-scale particles of arbitrary structure and shape. The main idea behind DDA is to represent scattering particles by arrays of small dipoles located at the nodes of rectangular lattices and compute the electric moments of these

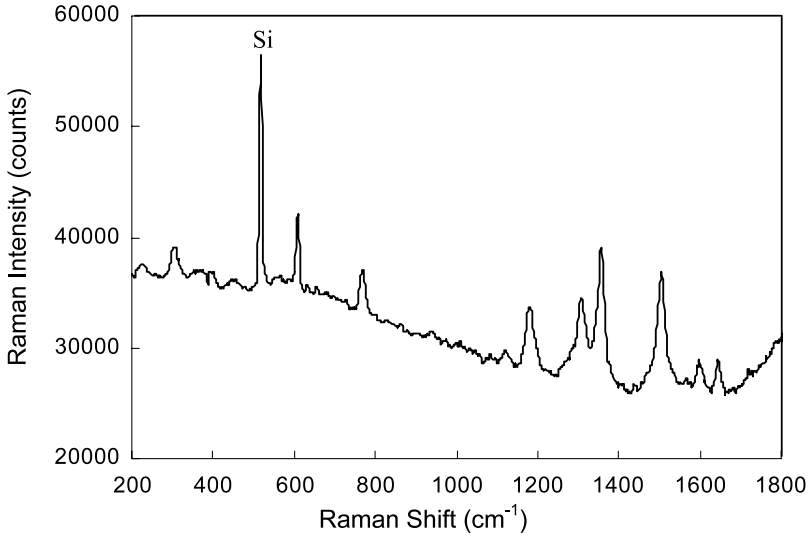

Figure 3. SERS spectrum of R6G adsorbed on a 200 nm period array of nanoprisms of 20 nm-thick Ag with 2.5 nm Cr adhesion layer.

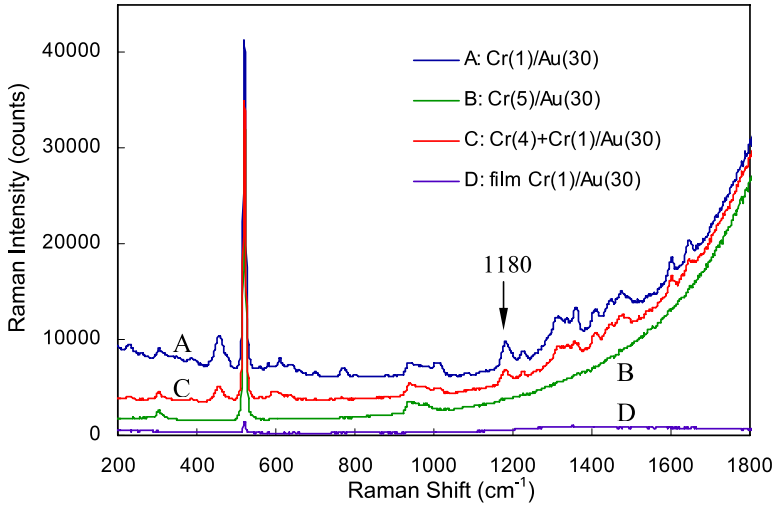

(a)

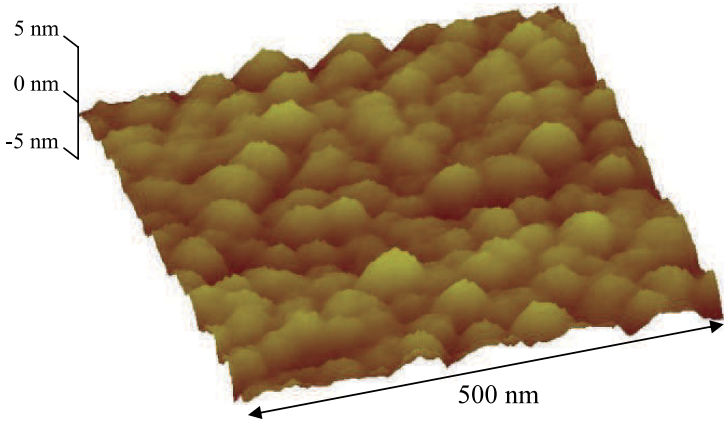

(b)

Figure 4. (a) SERS spectra of R6G adsorbed on a continuous film of Cr(1nm)/Au(30nm) and three nanoprism arrays as described in the text; (b) AFM image of the continuous film Cr(1 nm)/Au(30 nm) deposited on a flat silicon wafer showing a surface roughness of about 2 nm. The topographies for the films of Cr(5 nm)/Au(30 nm) and Cr(4 nm) + Cr(1 nm)/Au(30 nm) are similar.

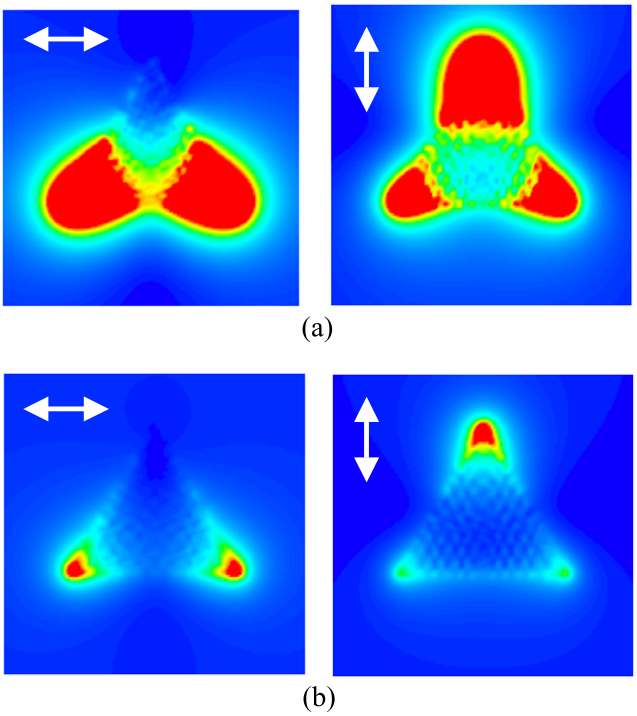

Figure 5. Near field of a freestanding 20 nm-thick Ag nanoprism without (a) and with (b) a 5 nm Cr adhesion layer calculated by DDA at $\lambda = 775$ nm. The arrow indicates the polarization of the incident light.

dipoles induced by an incident electromagnetic wave. Its main advantage over other numerical algorithms such as finite-difference time-domain (FDTD) is that only the domain of interest (the scatters) has to be discretized; the polarizabilities at each node of the mesh are then used in order to compute the electric field at each point of the space. As shown in figure 5(a), the near field for a freestanding Ag nanoprism with an edge length of 100 nm and a thickness of 20 nm is greatly enhanced at the sharp corners of the nanoprism. However, the near field drops significantly with the addition of 5 nm of Cr (figure 5(b)).

To study further the influence of the SiO_2 substrate, the Cr adhesion layer, the inter-prism coupling and the nanoprism thickness, we calculated the absorption efficiency (absorption cross-section divided by metal surface area) for nanoprisms with various configurations (figure 6), which indicates that:

(1) the surface plasmon dipolar resonant wavelength of a single freestanding nanoprism of 20 nm-thick Ag is around 720 nm, while those that are multipolar of order $l = 2$ and 3 lie between 400 and 500 nm with much weaker peaks;
(2) the addition of a 5 nm Cr adhesion layer reduces significantly the absorption efficiency;
(3) the effect of a SiO_2 substrate is to red-shift the (dipolar) resonant wavelength by about 100 nm;
(4) thicker Ag (60 nm) will decrease the resonant wavelength with little influence on absorption efficiency (but the absorption would decrease rapidly for Ag thinner than ∼10 nm);

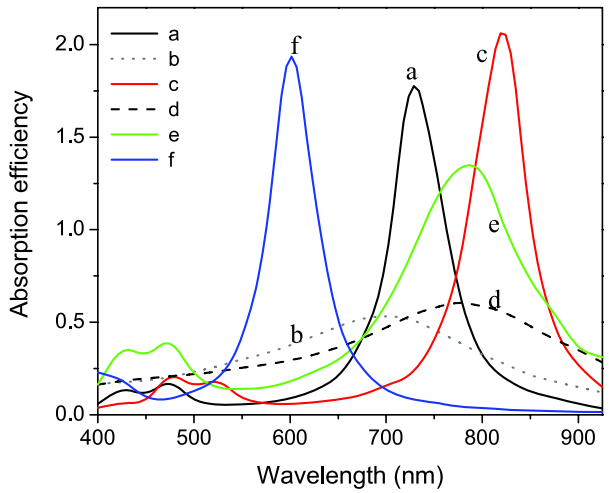

Figure 6. Absorption spectra obtained by DDA calculation of nanoprisms with various configurations: (a) Ag 20 nm, (b) Cr(5 nm)/Ag(20 nm), (c) SiO_2/Ag(20 nm), (d) SiO_2/Cr(5 nm)/Ag(20 nm), (e) 2 × 2 array Ag 20 nm, (f) Ag 60 nm.

(5) the 2×2 nanoprism array has a higher resonant wavelength and broader spectral peak than that of a single nanoprism due to inter-prism coupling, and the difference would depend on the spacing between adjacent nanoprisms.

Putting it all together, the fabricated 200 nm period nanoprism array of 20 nm Ag with a 2.5 nm Cr adhesion layer on a SiO_2 substrate is estimated to have a resonant wavelength of about 830 nm. However, as the corners of the nanoprisms are slightly rounded, the resonant wavelength of the fabricated nanoprism array should be blue-shifted below 800 nm [8, 16], thus matching well with the laser excitation wavelength (785 nm) used in our Raman system.

5. Conclusions

The fabrication of metallic nanoprisms over a large area has been demonstrated using NIL, wet and dry etching, and metal evaporation and liftoff, which are all low-cost processes. The method produces periodic nanoprism arrays with homogeneous size, shape and height. Silver and gold nanoprism arrays with a period of 200 nm and an edge length of 100 nm have been fabricated and tested as effective substrates for SERS detection of R6G molecules. Numerical calculations using a DDA algorithm confirmed the great enhancement of the electric field near the sharp nanoprism corners, as well as the detrimental effect of the thin chromium adhesion layer on localized surface plasmon resonance. In addition, the current approach can be used to fabricate non-equilateral nanoprisms and 3D nanopyramid arrays, and it can readily be extended to other metals. The modification of the current process in order to fabricate bowtie structures (two nanoprisms facing each other) for higher SERS enhancement [17] is underway.

References

[1] Jensen T R, Malinsky M D, Haynes C L and Van Duyne R P 2000 *J. Phys. Chem.* B **104** 10549

[2] Nelayah J, Kociak M, Stephan O, Garcia de Abajo F J, Tence M, Henrard L, Taverna D, Pastoriza-Santos I, Liz-Marzan L M and Colliex C 2007 *Nat. Phys.* **3** 348
[3] Kneipp K, Kneipp H, Itzkan I, Dasari R R and Feld M S 2002 *J. Phys.: Condens. Matter* **14** R597
[4] Moskovits M 2005 *J. Raman Spectrosc.* **36** 485
[5] Haes A J, Zou S, Schatz G C and Van Duyne R P 2004 *J. Phys. Chem.* B **108** 109
[6] Metraux G S and Mirkin C A 2005 *Adv. Mater.* **17** 412
[7] Jiang X, Zeng Q and Yu A 2006 *Nanotechnology* **17** 4929
[8] Jin R, Cao Y, Mirkin C A, Kelly K L, Schatz G C and Zheng J G 2001 *Science* **294** 1901
[9] Bastys V, Pastoriza-Santos I, Rodriguez-Gonzalez B, Vaisnoras R and Liz-Marzan L M 2006 *Adv. Funct. Mater.* **16** 766
[10] Schmidt J P, Cross S E and Buratto S K 2004 *J. Chem. Phys.* **121** 10657
[11] Sherry L J, Jin R, Mirkin C A, Schatz G C and Van Duyne R P 2006 *Nano Lett.* **6** 2060
[12] Draine B T 1988 *Astrophys. J.* **333** 848
[13] Purcell E M and Pennypacker C R 1973 *Astrophys. J.* **186** 705
[14] Yurkin M A, Maltsev V P and Hoekstra A G 2007 *J. Quant. Spectrosc. Radiat. Transf.* **106** 546
[15] Yang W H, Schatz G C and Van Duyne R P 1995 *J. Chem. Phys.* **103** 869
[16] Shuford K L, Ratner M A and Schatz G C 2005 *J. Chem. Phys.* **123** 114713
[17] Schuck P J, Fromm D P, Sundaramurthy A, Kino G S and Moerner W E 2005 *Phys. Rev. Lett.* **94** 017402